Realizing Synthetic Dimensions and Artificial Magnetic Flux in a Trapped-Ion Quantum Simulator

Y. Wang,[1,*] Y.-K. Wu,[1,2,*] Y. Jiang,[1] M.-L. Cai,[3] B.-W. Li,[3] Q.-X. Mei,[3] B.-X. Qi,[1] Z.-C. Zhou,[1,2] and L.-M. Duan[1,2,4,†]

[1]*Center for Quantum Information, Institute for Interdisciplinary Information Sciences, Tsinghua University, Beijing 100084, People's Republic of China*

[2]*Hefei National Laboratory, Hefei 230088, People's Republic of China*

[3]*HYQ Co., Ltd., Beijing 100176, People's Republic of China*

[4]*New Cornerstone Science Laboratory, Beijing 100084, People's Republic of China*

(Received 28 July 2023; revised 12 December 2023; accepted 29 February 2024; published 25 March 2024)

Synthetic dimension is a potent tool in quantum simulation of topological phases of matter. Here we propose and demonstrate a scheme to simulate an anisotropic Harper-Hofstadter model with controllable magnetic flux on a two-leg ladder using the spin and motional states of a single trapped ion. We verify the successful simulation of this model by comparing the measured dynamics with theoretical predictions under various coupling strength and magnetic flux, and we observe the chiral motion of wave packets on the ladder as evidence of the topological chiral edge modes. We develop a quench path to adiabatically prepare the ground states for varying magnetic flux and coupling strength, and we measure the chiral current on the ladder for the prepared ground states, which allows us to probe the quantum phase transition between the Meissner phase and the vortex phase. Our work demonstrates the trapped ion as a powerful quantum simulation platform for topological quantum matter.

DOI: 10.1103/PhysRevLett.132.130601

Topological quantum matter shows novel phases of materials such as topological insulators, topological superconductors, and quantum Hall phases that are characterized by global properties rather than local order parameters [1–3]. Spatial dimensionality plays a crucial role in the classification of topological quantum matter. Together with the symmetry of the system, it determines a periodic table for the topological invariants [3]. Although rich topological properties are predicted for high-dimensional systems [4–7], to observe them in three-dimensional materials in the laboratory can be a challenge. An appealing alternative approach has been taken to implement these models through quantum simulation, with the extra dimensions synthesized from the various degrees of freedom of the system [8–10]. Apart from exploring high-dimensional physics, synthetic dimensions also provide a convenient way to engineer artificial gauge fields on the simulated lattice through the site-dependent hopping, which gives nonzero magnetic flux in each unit cell. Such an artificial magnetic field can be much stronger than those generated in real materials and can work for even neutral particles, thus allowing efficient quantum simulation of topological states like quantum Hall phases [10–13].

Various schemes have been taken to create synthetic dimensions, such as the internal energy levels or discrete momentum states of cold neutral atoms [11,12] and different frequencies or orbital angular momenta in photonics [13]. Fock states of oscillation modes are also proposed as a synthetic dimension [14], which opens up a new direction to extend the dimensionality with large number of sites and is realized recently for neutral atoms by modulating the trap potential [15]. Here, we propose and demonstrate a scheme to implement synthetic dimensions and artificial magnetic flux in ion trap using the laser-coupled internal and motional degrees of freedom. Recently, synthetic dimensions have also been achieved using microwave photons with the help of a superconducting qubit [16]. However, there the qubit is to intermediate the transition between different microwave cavities and is not regarded as an additional dimension, thus the qubit and n photon modes give a total synthetic dimension of $n-1$. In comparison, in our scheme both spin and phonon states are regarded as independent dimensions and we get $n+1$ synthetic dimensions from a qubit and n phonon modes.

As one of the leading platforms for quantum information processing and quantum simulation, ion trap naturally hosts high-fidelity initialization, manipulation, and readout of phonon states [17] with the help of ions' internal levels through laser-induced phonon sideband transitions and spin-dependent forces. Quantum simulation of spin-boson-coupled systems has been performed for quantum Rabi model on a single trapped ion [18–20] and for Hubbard-like models on up to tens of ions [21–25]. Recently, joint tomography of the spin and phonon states has also been demonstrated [26]. These tools enable our measurements of population and current on the synthetic

lattice sites. Specifically, here we achieve a two-leg ladder via the spin and motional states of a single trapped ion, and simulate an anisotropic Harper-Hofstadter (HH) model [14] with fully controllable magnetic flux. After verifying the model by comparing with theoretical predictions under representative parameters, we further observe the topological effect of the chiral motion of a wave packet, and demonstrate the quantum phase transition between the Meissner phase and the vortex phase of the HH model from adiabatically prepared ground states. Our work showcases the ion trap as a powerful quantum simulator, and may be extended to higher synthetic dimensions for diverse topological effects.

Scheme.—Consider a two-leg ladder shown in Fig. 1 where the x direction is represented by the phonon number $|n\rangle$ and the y direction by the spin states $|\uparrow\rangle$ and $|\downarrow\rangle$. Our target is to simulate an anisotropic HH model with Hamiltonian [14]

$$\begin{aligned} H_{\mathrm{HH}} &= \Delta a^\dagger a - J_y\sigma_x - J_x\left[ae^{i(\varphi\sigma_z+\theta)} + a^\dagger e^{-i(\varphi\sigma_z+\theta)}\right] \\ &= \Delta a^\dagger a - J_y\sigma_x - J_x\cos\varphi(ae^{i\theta} + a^\dagger e^{-i\theta}) \\ &\quad - iJ_x\sin\varphi\sigma_z(ae^{i\theta} - a^\dagger e^{-i\theta}), \end{aligned} \tag{1}$$

where $\sigma_{x,y,z}$ are Pauli operators on spin states and a ($a^\dagger$) is the annihilation (creation) operator of the phonon. In the Fock basis, we have a constant hopping J_y in the y direction and a phonon-dependent hopping strength $J_x\sqrt{n+1}$ in the x direction between phonon numbers n and $n+1$. Furthermore, there is a spin-dependent Peierls phase [27] of $\pm\varphi$ in the hopping amplitude which generates a magnetic flux of $\Phi = 2\varphi$ in each unit cell, and a spin-independent phase θ which corresponds to a shift in the momentum space. Δ represents a linear potential along the x direction and can be used to study Hall transport [14].

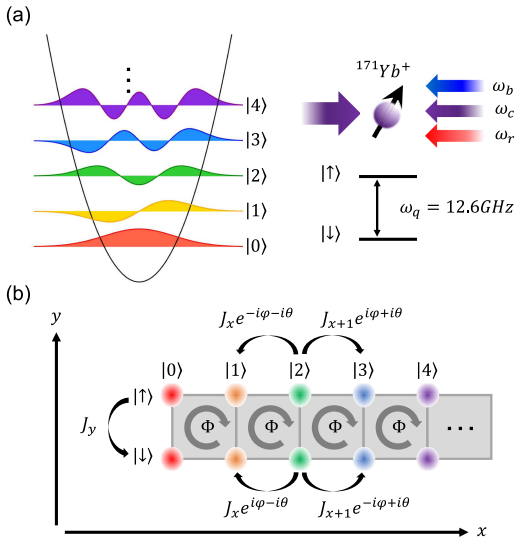

FIG. 1. Experimental scheme. (a) We use the spin and a phonon mode of a trapped ion to simulate the two-leg ladder model. Two counterpropagating laser beams are shined on the ion to drive three pairs of Raman transitions near the carrier and the blue and the red motional sidebands. (b) The simulated two-leg ladder model. Its x direction is represented by the phonon number $|n\rangle$ and the y direction by the spin states $|\uparrow\rangle$ and $|\downarrow\rangle$. The carrier driving provides the coupling along the spin direction, while the driving near the two motional sidebands generates a spin-dependent force, which translates into the site-dependent coupling along the phonon direction with an adjustable magnetic flux in a suitable frame of reference.

The Hamiltonian in Eq. (1) contains a detuning in the phonon mode, a resonant driving on the spin transition, and spin-independent and spin-dependent forces. The spin-dependent force is widely used in ion trap, generated from bichromatic laser driving [28]. In principle, the spin-independent force can be created by an oscillating electric field at the frequency of the phonon mode [17]. However, such a force, acting solely on the motional state, is more difficult to control and calibrate than the laser-induced one, therefore we choose the implement the Hamiltonian in Eq. (1) by the spin-dependent force via suitable unitary transform. Specifically, we consider a unitary $U = R_x(\pi/2) \otimes D(J_x e^{-i\theta}\cos\varphi/\Delta)$, where $R_x(\pi/2)$ is a rotation along σ_x by $\pi/2$, and $D(\alpha) \equiv \exp(\alpha a^\dagger - \alpha^* a)$ is the displacement operator. In the transformed frame, the Hamiltonian $H_0 = U^\dagger H_{\mathrm{HH}} U = \Delta a^\dagger a + (\Omega_c/2)\sigma_x - i(\eta\Omega_s/2)\sigma_y(ae^{i\theta} - a^\dagger e^{-i\theta})$ turns into a familiar form in ion trap quantum simulation [18,19], where we identify $\eta\Omega_s = 2J_x\sin\varphi$ and $\Omega_c = -2J_y$ (see Supplemental Material [29]). To simulate the dynamics of an initial state $|\psi\rangle$ under H_{HH}, we prepare $U^\dagger|\psi\rangle$ where the displacement can be realized by a spin-dependent force with a suitable initial spin state. After time evolution under H_0, we further need a unitary U on the final state, which can be absorbed into the blue or red sideband evolution when measuring the phonon state [26,33].

First we verify the successful simulation of H_{HH} under various parameters from an initial product state of the spin and the phonon. Without a magnetic field [Fig. 2(a)], the spin and the phonon states evolve separately even though

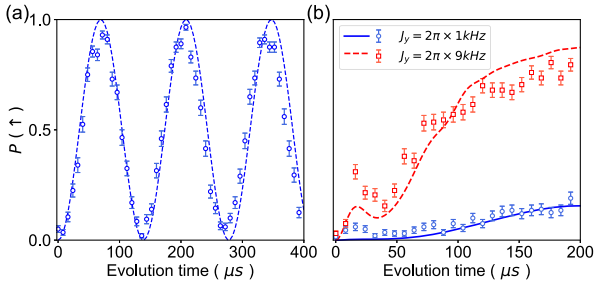

FIG. 2. Comparison of experimental and theoretical dynamics under various parameters for the HH Hamiltonian in Eq. (1) from an initial state $|\downarrow\rangle|\alpha = 2\rangle$. We choose $\Delta = 2\pi \times 2$ kHz and $\theta = \pi/2$. (a) $J_x = 2\pi \times 4$ kHz, $J_y = 2\pi \times 3.6$ kHz, and $\Phi = 2\varphi = 0$. (b) $J_x = 2\pi \times 6$ kHz, $\Phi = 2\varphi = \pi/2$ and various J_y.

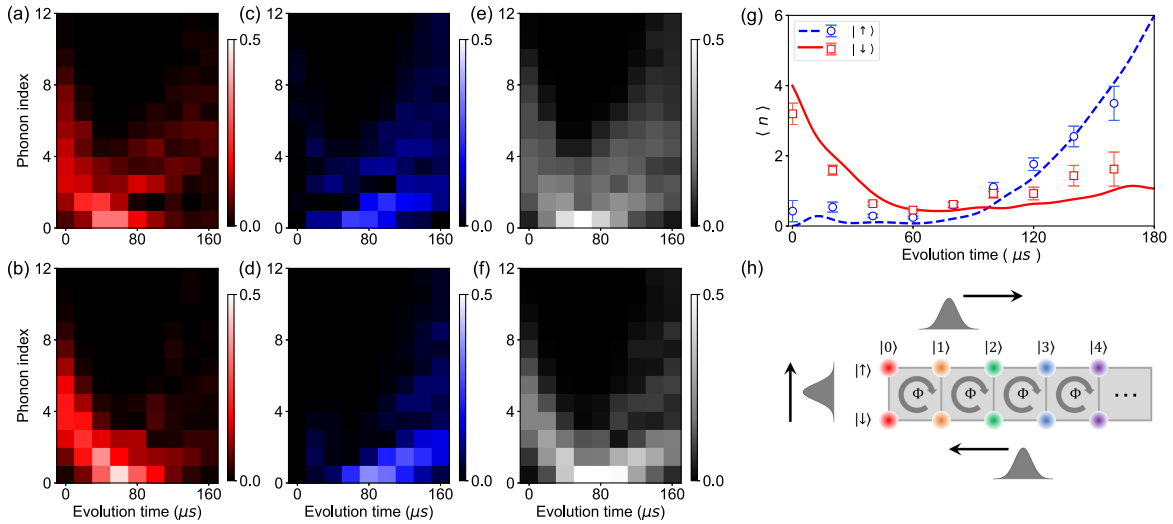

FIG. 3. Chiral motion of an initial wave packet $|\downarrow\rangle|\alpha = 2\rangle$ under the HH model with $\Delta = 2\pi \times 2$ kHz, $J_x = J_y = 2\pi \times 6$ kHz, $\Phi = 2\varphi = \pi/2$, and $\theta = \pi/2$. (a)–(f) Time evolution of phonon population in the lower leg ($|\downarrow\rangle$, first column), the upper leg ($|\uparrow\rangle$, second column) and their combination (third column). The experimental results (first row) agree well with the theoretical prediction (second row). (g) Time evolution of average phonon number in the lower and upper legs. (h) Schematic dynamics of a wave packet initially located on the lower leg centered around $\langle n\rangle = |\alpha|^2 = 4$. First it stays on the lower leg and moves to the left, then starts to transfer to the upper leg at the boundary $n = 0$, and finally moves to the right on the upper leg.

the couplings in both x and y directions are on, thus we observe a Rabi oscillation in the spin state. When a magnetic flux $\Phi = 2\varphi = \pi/2$ is turned on [Fig. 2(b)], the population transfer from $|\downarrow\rangle$ to $|\uparrow\rangle$ slows down due to the restriction of edge modes. Later we will see that the weak and the strong J_y correspond to the vortex phase and the Meissner phase, respectively. In all these situations, the measured spin dynamics agree reasonably well with the theoretical predictions, given that all these parameters are calibrated in advance and that there is no fitting parameters in the theoretical curves.

The topological property of the HH model can be reflected from its chiral edge states [1–3]. A two-leg (or few-leg) ladder is a minimal model to observe such chiral edge modes [34–40] with its two energy bands showing opposite chirality: In each band, particles on one leg tends to move in one direction and those on the other leg tends to move in the other direction. Such a chiral motion still persists in the anisotropic HH model [14]. As we show in Fig. 3, for an initial wave packet $|\downarrow\rangle|\alpha = 2\rangle$ on the lower leg of the ladder, originally it stays on the lower leg and moves to the left, and then transfers to the upper leg once it hits the boundary at $n = 0$. Finally the wave packet on the upper leg moves to the right.

The chiral edge modes can be regarded as the Meissner effect where the edge current screens out the external magnetic field up to a critical value. As the magnetic field increases, a quantum phase transition occurs from the Meissner phase into a vortex phase [35,41]. This is most easily seen from an isotropic and homogeneous two-leg ladder HH model with $\Delta = 0$ and $L \to \infty$ sites along the x direction. For simplicity, below we set the global phase $\theta = 0$. Defining momentum basis $|q, \uparrow(\downarrow)\rangle \equiv \sum_n e^{iqn}|n, \uparrow(\downarrow)\rangle/\sqrt{L}$, where $q = 2\pi m/L$ $(m = -L/2, -L/2+1, \ldots, L/2-1)$, the Hamiltonian can be expressed as $H = -2J_x\sum_q[|q,\uparrow\rangle\langle q,\uparrow|\cos(q+\varphi) + |q,\uparrow\rangle\langle q,\downarrow|\cos(q-\varphi)] - J_y\sum_q(|q,\uparrow\rangle\langle q,\downarrow| + \text{H.c.})$. We plot its typical energy band structure in Fig. 4(a) for weak and strong magnetic field at $J_x = J_y = J$. At weak magnetic field (dashed curves), the lower band has a unique ground state at $q = 0$ as an equal superposition of all the sites. This gives a chiral current $j_c \equiv i\sum_n(|n+1,\uparrow\rangle\langle n,\uparrow|e^{-i\varphi} - |n+1,\downarrow\rangle\langle n,\downarrow|e^{i\varphi}) + \text{H.c.}$ increasing with the magnetic field $\langle j_c\rangle = 2\sin(\varphi/2)$. On the other hand, at strong magnetic field (solid curves), the lower band shows two degenerate ground states close to $q = \pm\varphi$. These momentum states are out-of-phase with the definition of the chiral current, thus a reduction in $\langle j_c\rangle$ as φ further increases. As shown in Fig. 4(c), for the isotropic HH model (green solid curve), sharp nonanalytical behavior in j_c can be seen near the critical magnetic flux φ_c.

To observe this phase transition, we adiabatically prepare the ground state of Eq. (1) and measure its chiral current (see Supplemental Material [29]). For any desired parameters, we start from $J_x = 0$ such that the initial ground state is given by the product state $|+\rangle|0\rangle$ of the spin and the phonon modes when $J_y > 0$ and $\Delta > 0$. Then we gradually turn up J_x and expect the system to stay in the ground state under slow quench. However, note that as we vary the parameters, the unitary transform U also becomes time dependent and will cause a correction term of $-iU\partial U^\dagger/\partial t$ in the effective Hamiltonian. In the adiabatic limit, this

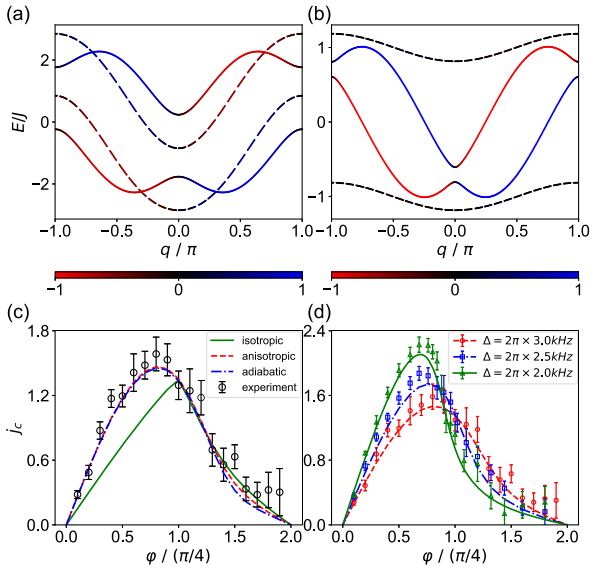

FIG. 4. Quantum phase transition in the HH model. (a) Energy band structure for an isotropic HH model at $\Delta = 0$ and $J_x = J_y = J$ under small ($\varphi = \pi/8$, dashed curves, Meissner phase) or large ($\varphi = 3\pi/8$, solid curves, vortex phase) magnetic flux, respectively. The color represents the spin component $\langle \sigma_z \rangle$ of the eigenstates. (b) Energy band structure for an isotropic HH model at $\Delta = 0$ and $\varphi = \pi/4$ under large ($J_x = 0.1J$, $J_y = J$, dashed curves, Meissner phase) or small ($J_x = 0.5J$, $J_y = 0.1J$, solid curves, vortex phase) coupling ratio, respectively. (c) Chiral current for the adiabatically prepared ground state at $\Delta = 2\pi \times 3$, $J_x = 2\pi \times 6$, and $J_y = 2\pi \times 9$ kHz (black circles for experiment and blue dash-dotted curve for theory), the ideal ground state for the anisotropic HH model (red dashed curve) and the isotropic HH model (green solid curve) vs magnetic flux φ. (d) Similar plot as (c) under various detuning Δ. Dots represent experimental data and curves represent ideal ground states for the anisotropic HH model.

correction term will be small, but even for a finite quench rate, its effect can be cancelled by suitable modification in the quench parameters $\alpha(t)$ (see Supplemental Material [29]). In Fig. 4(c) we show the experimental data as the black circles and the theoretical results for an anisotropic HH model as the red dashed curve. Similar to the isotropic HH model (green solid curve), we observe an initial linear increase in j_c vs φ, a peak near the expected critical magnetic flux, and a decrease in j_c as φ further increases. Here the initial slope of the curve is higher than the isotropic model because of the stronger coupling in the x direction by $\sqrt{n}$ and a corresponding modification in the definition of the chiral current $j_c \equiv i\sigma_z a^\dagger e^{-i\varphi\sigma_z}$ [14]. Also note that the peak in the transition signal is broader than the ideal isotropic model. This can be explained by the finite size effect of a bounded number of phonons as we describe below.

In order to cancel the spin-independent force in the Hamiltonian [Eq. (1)], here we choose a nonzero detuning Δ of the phonon mode. Furthermore, to adiabatically prepare the ground state, we require $\Delta > 0$. This corresponds to a constant force along the simulated two-leg ladder, and helps to keep the phonon number bounded, both in the ground state and in the dynamics [14]. Strictly speaking, an equilibrium phase cannot be defined under such a constant force, not to mention a phase transition. However, if we gradually reduce Δ and extrapolate to the limit $\Delta \to 0$, we can still expect a nonanalytical behavior in analogue to the thermodynamic limit in an ordinary phase transition. As shown in Fig. 4(d), when we decrease Δ from $2\pi \times 3$ to $2\pi \times 2$ kHz, the curve for the chiral current does get sharper. Also note that the transition point is shifting to smaller φ as Δ decreases. This is because when Δ decreases, the average phonon number increases so that effectively the coupling J_x also increases with $\sqrt{n}$. As we shown in Supplemental Material [29], with a suitable rescaling in the parameter J_y and the observable j_c, these curves will converge to a nonanalytical curve in the limit $\Delta \to 0$, thus proving a quantum phase transition.

Another way to probe the phase transition, which is used in previous experiments without the freedom to arbitrarily control the magnetic flux, is to scan the ratio J_y/J_x under a fixed $\Phi = 2\varphi = \pi/2$. Again we can understand this phase transition from the energy band structure of an isotropic HH model at $\Delta = 0$. As shown in Fig. 4(b), similar to the previous case, when $J_y/J_x \gg 1$ (dashed curves), we get the Meissner phase with a unique ground state at $q = 0$, so that the chiral current saturates at $\langle j_c \rangle = 2\sin(\varphi/2)$. In comparison, when $J_y/J_x \ll 1$ (solid curves), we get the vortex phase with two degenerate ground states near $q = \pm\varphi$, giving vanishing chiral current. However, if we follow a similar procedure to adiabatically prepare the ground state and measure the chiral current for various J_y/J_x, as shown in Supplemental Material [29], although the experimental data still agrees with the theoretical prediction for the anisotropic HH model, the transition signal near the critical ratio J_y/J_x is not visible, and finally for sufficiently large J_y/J_x, the chiral current will saturates at J_x/Δ. Therefore we conclude that for this anisotropic model with increasing hopping proportional to $\sqrt{n}$, scanning the magnetic flux is the preferable way to probe this quantum phase transition.

Discussion.—Our work can be readily generalized to four dimensions with a single spin and the three spatial oscillation modes. Through laser-induced spin-dependent forces on these three modes, magnetic flux between these motional directions and the spin direction can be freely controlled. On the other hand, to engineer flux between the motional directions is more complicated and may require nonlinear interactions between these modes. It is also possible to generalize the synthetic dimension to multiple ions as we discuss in Supplemental Material [29].

Also note that, when studying the quantum phase transition, we take the limit $\Delta \to 0$ in a similar way as the previously studied quantum phase transition in the quantum Rabi model without a thermodynamic limit,

where the frequency ratio between the spin and the bosonic modes is used for finite size scaling instead of the particle number for an ordinary phase transition [19,42]. On the other hand, in this work there is a clear correspondence between the detuning Δ and the number of sites in the anisotropic HH model. Therefore, our work can make a bridge between these two types of phase transitions and can help deepen the understanding of their physical essence.

This work was supported by Innovation Program for Quantum Science and Technology (2021ZD0301601), Tsinghua University Initiative Scientific Research Program, and the Ministry of Education of China. L.-M. D. acknowledges in addition support from the New Cornerstone Science Foundation through the New Cornerstone Investigator Program. Y.-K. W. acknowledges in addition support from National Key Research and Development Program of China (2020YFA0309500), Tsinghua University Dushi program and the start-up fund.

*These authors contributed equally to this letter.
†lmduan@tsinghua.edu.cn

[1] M. Z. Hasan and C. L. Kane, Colloquium: Topological insulators, Rev. Mod. Phys. **82**, 3045 (2010).
[2] Xiao-Liang Qi and Shou-Cheng Zhang, Topological insulators and superconductors, Rev. Mod. Phys. **83**, 1057 (2011).
[3] Ching-Kai Chiu, Jeffrey C. Y. Teo, Andreas P. Schnyder, and Shinsei Ryu, Classification of topological quantum matter with symmetries, Rev. Mod. Phys. **88**, 035005 (2016).
[4] Shou-Cheng Zhang and Jiangping Hu, A four-dimensional generalization of the quantum Hall effect, Science **294**, 823 (2001).
[5] Xiao-Liang Qi, Taylor L. Hughes, and Shou-Cheng Zhang, Topological field theory of time-reversal invariant insulators, Phys. Rev. B **78**, 195424 (2008).
[6] Alexei Kitaev, Periodic table for topological insulators and superconductors, AIP Conf. Proc. **1134**, 22 (2009).
[7] Andreas P. Schnyder, Shinsei Ryu, Akira Furusaki, and Andreas W. W. Ludwig, Classification of topological insulators and superconductors, AIP Conf. Proc. **1134**, 10 (2009).
[8] O. Boada, A. Celi, J. I. Latorre, and M. Lewenstein, Quantum simulation of an extra dimension, Phys. Rev. Lett. **108**, 133001 (2012).
[9] A. Celi, P. Massignan, J. Ruseckas, N. Goldman, I. B. Spielman, G. Juzeliunas, and M. Lewenstein, Synthetic gauge fields in synthetic dimensions, Phys. Rev. Lett. **112**, 043001 (2014).
[10] Tomoki Ozawa and Hannah M. Price, Topological quantum matter in synthetic dimensions, Nat. Rev. Phys. **1**, 349 (2019).
[11] Dan-Wei Zhang, Yan-Qing Zhu, Y. X. Zhao, Hui Yan, and Shi-Liang Zhu, Topological quantum matter with cold atoms, Adv. Phys. **67**, 253 (2018).
[12] N. R. Cooper, J. Dalibard, and I. B. Spielman, Topological bands for ultracold atoms, Rev. Mod. Phys. **91**, 015005 (2019).
[13] Tomoki Ozawa, Hannah M. Price, Alberto Amo, Nathan Goldman, Mohammad Hafezi, Ling Lu, Mikael C. Rechtsman, David Schuster, Jonathan Simon, Oded Zilberberg, and Iacopo Carusotto, Topological photonics, Rev. Mod. Phys. **91**, 015006 (2019).
[14] Hannah M. Price, Tomoki Ozawa, and Nathan Goldman, Synthetic dimensions for cold atoms from shaking a harmonic trap, Phys. Rev. A **95**, 023607 (2017).
[15] Christopher Oliver, Aaron Smith, Thomas Easton, Grazia Salerno, Vera Guarrera, Nathan Goldman, Giovanni Barontini, and Hannah M. Price, Bloch oscillations along a synthetic dimension of atomic trap states, Phys. Rev. Res. **5**, 033001 (2023).
[16] Jinfeng Deng, Hang Dong, Chuanyu Zhang, Yaozu Wu, Jiale Yuan, Xuhao Zhu, Feitong Jin, Hekang Li, Zhen Wang, Han Cai, Chao Song, H. Wang, J. Q. You, and Da-Wei Wang, Observing the quantum topology of light, Science **378**, 966 (2022).
[17] D. Leibfried, R. Blatt, C. Monroe, and D. Wineland, Quantum dynamics of single trapped ions, Rev. Mod. Phys. **75**, 281 (2003).
[18] Dingshun Lv, Shuoming An, Zhenyu Liu, Jing-Ning Zhang, Julen S. Pedernales, Lucas Lamata, Enrique Solano, and Kihwan Kim, Quantum simulation of the quantum Rabi model in a trapped ion, Phys. Rev. X **8**, 021027 (2018).
[19] M.-L. Cai, Z.-D. Liu, W.-D. Zhao, Y.-K. Wu, Q.-X. Mei, Y. Jiang, L. He, X. Zhang, Z.-C. Zhou, and L.-M. Duan, Observation of a quantum phase transition in the quantum Rabi model with a single trapped ion, Nat. Commun. **12**, 1126 (2021).
[20] R. Gerritsma, G. Kirchmair, F. Zähringer, E. Solano, R. Blatt, and C. F. Roos, Quantum simulation of the Dirac equation, Nature (London) **463**, 68 (2010).
[21] Q.-X. Mei, B.-W. Li, Y.-K. Wu, M.-L. Cai, Y. Wang, L. Yao, Z.-C. Zhou, and L.-M. Duan, Experimental realization of the Rabi-Hubbard model with trapped ions, Phys. Rev. Lett. **128**, 160504 (2022).
[22] Kenji Toyoda, Yuta Matsuno, Atsushi Noguchi, Shinsuke Haze, and Shinji Urabe, Experimental realization of a quantum phase transition of polaritonic excitations, Phys. Rev. Lett. **111**, 160501 (2013).
[23] Ryutaro Ohira, Shota Kume, Kyoichi Takayama, Silpa Muralidharan, Hiroki Takahashi, and Kenji Toyoda, Blockade of phonon hopping in trapped ions in the presence of multiple local phonons, Phys. Rev. A **103**, 012612 (2021).
[24] S. Debnath, N. M. Linke, S.-T. Wang, C. Figgatt, K. A. Landsman, L.-M. Duan, and C. Monroe, Observation of hopping and blockade of bosons in a trapped ion spin chain, Phys. Rev. Lett. **120**, 073001 (2018).
[25] B.-W. Li, Q.-X. Mei, Y.-K. Wu, M.-L. Cai, Y. Wang, L. Yao, Z.-C. Zhou, and L.-M. Duan, Observation of non-Markovian spin dynamics in a Jaynes-Cummings-Hubbard model using a trapped-ion quantum simulator, Phys. Rev. Lett. **129**, 140501 (2022).
[26] M-L Cai, Y-K Wu, Q-X Mei, W-D Zhao, Y Jiang, L Yao, L He, Z-C Zhou, and L-M Duan, Observation of supersymmetry and its spontaneous breaking in a trapped ion quantum simulator, Nat. Commun. **13**, 3412 (2022).
[27] Rudolph Peierls, Zur theorie des diamagnetismus von Leitungselektronen, Z. Phys. **80**, 763 (1933).

[28] P. C. Haljan, K.-A. Brickman, L. Deslauriers, P. J. Lee, and C. Monroe, Spin-dependent forces on trapped ions for phase-stable quantum gates and entangled states of spin and motion, Phys. Rev. Lett. **94**, 153602 (2005).

[29] See Supplemental Material at http://link.aps.org/supplemental/10.1103/PhysRevLett.132.130601 for details about our scheme to simulate the time-dependent HH model, the way to measure the chiral current and the spin-dependent phonon population, and further discussions about the quantum phase transition in the anisotropic HH model and about generalizing the scheme to multiple ions, which include Refs. [30–32].

[30] C. Monroe, W. C. Campbell, L.-M. Duan, Z.-X. Gong, A. V. Gorshkov, P. W. Hess, R. Islam, K. Kim, N. M. Linke, G. Pagano, P. Richerme, C. Senko, and N. Y. Yao, Programmable quantum simulations of spin systems with trapped ions, Rev. Mod. Phys. **93**, 025001 (2021).

[31] A. C. Wilson, Y. Colombe, K. R. Brown, E. Knill, D. Leibfried, and D. J. Wineland, Tunable spin–spin interactions and entanglement of ions in separate potential wells, Nature (London) **512**, 57 (2014).

[32] S. Korenblit, D. Kafri, W. C. Campbell, R. Islam, E. E. Edwards, Z.-X. Gong, G.-D. Lin, L.-M. Duan, J. Kim, K. Kim, and C. Monroe, Quantum simulation of spin models on an arbitrary lattice with trapped ions, New J. Phys. **14**, 095024 (2012).

[33] D. Kienzler, C. Flühmann, V. Negnevitsky, H.-Y. Lo, M. Marinelli, D. Nadlinger, and J. P. Home, Observation of quantum interference between separated mechanical oscillator wave packets, Phys. Rev. Lett. **116**, 140402 (2016).

[34] Dario Hügel and Belén Paredes, Chiral ladders and the edges of quantum Hall insulators, Phys. Rev. A **89**, 023619 (2014).

[35] Marcos Atala, Monika Aidelsburger, Michael Lohse, Julio T Barreiro, Belén Paredes, and Immanuel Bloch, Observation of chiral currents with ultracold atoms in bosonic ladders, Nat. Phys. **10**, 588 (2014).

[36] M. Mancini, G. Pagano, G. Cappellini, L. Livi, M. Rider, J. Catani, C. Sias, P. Zoller, M. Inguscio, M. Dalmonte, and L. Fallani, Observation of chiral edge states with neutral fermions in synthetic Hall ribbons, Science **349**, 1510 (2015).

[37] B. K. Stuhl, H.-I. Lu, L. M. Aycock, D. Genkina, and I. B. Spielman, Visualizing edge states with an atomic Bose gas in the quantum Hall regime, Science **349**, 1514 (2015).

[38] M. Eric Tai, Alexander Lukin, Matthew Rispoli, Robert Schittko, Tim Menke, Dan Borgnia, Philipp M. Preiss, Fabian Grusdt, Adam M. Kaufman, and Markus Greiner, Microscopy of the interacting Harper-Hofstadter model in the two-body limit, Nature (London) **546**, 519 (2017).

[39] Fangzhao Alex An, Eric J. Meier, and Bryce Gadway, Direct observation of chiral currents and magnetic reflection in atomic flux lattices, Sci. Adv. **3**, e1602685 (2017).

[40] Yuqing Li, Jiahui Zhang, Yunfei Wang, Huiying Du, Jizhou Wu, Wenliang Liu, Feng Mei, Jie Ma, Liantuan Xiao, and Suotang Jia, Atom-optically synthetic gauge fields for a noninteracting Bose gas, Light Sci. Appl. **11**, 13 (2022).

[41] E. Orignac and T. Giamarchi, Meissner effect in a bosonic ladder, Phys. Rev. B **64**, 144515 (2001).

[42] Myung-Joong Hwang, Ricardo Puebla, and Martin B. Plenio, Quantum phase transition and universal dynamics in the Rabi model, Phys. Rev. Lett. **115**, 180404 (2015).